SF2A 2016
C. Reylé, J. Richard, L. Cambrésy, M. Deleuil, E. Pécontal, L. Tresse and I. Vauglin (eds)

WHICH MECHANISM FOR GAMMA-RAY FLARES OF THE CRAB NEBULA ?

T. Akramov[1] and H. Baty

Abstract. We report preliminary results using two dimensional (2D) classical MagnetoHydroDynamic (MHD) simulations with the aim to investigate the physical mechanism underlying gamma-ray flares. We explore the explosive reconnection mechanism proposed by Baty et al. (2013) in order to confirm its ability to produce flares when located in the stripped wind region. In particular, the time scale of the process is shown to be independent of the unkown dissipation, enforcing the robustness of the model. A considerable particle acceleration is also obtained, involving a potentially important non thermal contribution for the resulting synchrotron radiation.

Keywords: plasma - reconnection - high-energy - gamma-rays

1 Introduction

The Crab pulsar and its surrounding nebula is a well-known relic of a massive star that exploded in 1054 AD. The Crab nebula was generally believed to be a good standard candle in gamma rays. Recently, this view has been challenged by sudden increases in the gamma-ray flux in a narrow spectral band within a few hundred MeV, as observed in gamma-rays by Fermi/LAT. These flares are short but powerful; their duration is between a few hours and up to several days with a rising/falling time of a few hours/days [Striani et al. (2013)]. To date it is neither clear what mechanism powers these flares nor where exactly in the nebula they should be located.

Magnetic reconnection could be an efficient mechanism to explain these flares [Clausen-Brown & Lyutikov (2012)]. The tearing instability of current sheets is the simplest way of triggering magnetic reconnection [Lyutikov (2003)]. Recently, Baty et al. (2013) proposed an explosive mechanism based on the double tearing mode (DTM). The favoured site for the radiation emission corresponds to a region situated in the stripped wind close to the light cylinder radius ($r \simeq 50 r_L$). Indeed, the DTM is a magnetohydrodynamic (MHD) instability that is known to develop in multiple current sheets, as expected from the magnetic structure of pulsars magnetosphere with the presence of a current sheet wobbling around the equatorial plane [Coroniti (1990)].

The aim of our work is to explore into more detail the physical mechanism underlying the DTM mode, with a particular emphasis on the time scale giving the fast and explosive character of the process. This is investigated by means of two dimensional (2D) classical resistive MHD simulations. We also explore the consequences for particles using an independent test-particle acceleration code. Preliminary results are presented in this paper.

2 MHD model and numerical setup

We use the resistive MHD model in the non relativistic framework; and the two-dimensional cartesian geometry (x, y) is considered. The initial magnetic structure consists of a double Harris current sheet configuration in static equilibrium:

$$B_x = 0, B_y = B_0[1 - \tanh(\frac{x + x_0}{a}) + \tanh(\frac{x - x_0}{a})], \tag{2.1}$$

where a is the half-width of each current sheet and x_0 gives the location of the current sheets. An isothermal plasma with a small β-parameter is considered here as $\beta = 0.2$. We set the ratio of specific heats γ equal to $5/3$ and choose units such that the magnetic permeability is unity, $\mu_0 = 1$. We also set $B_0 = 1$ and $a = 0.2$ to

[1] Observatoire Astronomique de Strasbourg, Université de Strasbourg, CNRS, UMR 7550, 11 rue de l'université, F-67000 Strasbourg, France

define our normalization. The velocity is normalized by the characteristic Alfvén speed v_A given by $B_0/\sqrt{4\pi\rho_0}$ and we set $v_A = 1$. The current sheets are located at $x = \pm x_0$ with $x_0 = 0.5$. A divergence-free magnetic field ($\delta B \sim 10^{-3} B_0$) is used to perturb the system at the initial time. The simulations are carried out using the shock-capturing MPI-AMRVAC code with the finite-volume method [Porth et al. (2014)] in a square box of dimensions $[-2:2] \times [-2:2]$ including 960×960 grid cells. In order to investigate the scaling law of the explosive DTM growth, a high number of resistivity values (η) will be considered, η beeing here the parameter of the unkown magnetic dissipation.

In addition, we perform test-particle calculations to investigate particle acceleration mechanisms during the DTM evolution at the different MHD times. For the sake of simplicity, a single particle with an effective mass $m = 10 m_e$ is introduced (m_e being the electron mass). A standard second-order (Boris-Buneman) time integrator is used to solve the motion equation. The integration time is $t_{int} = 4.4 \times 10^3 \tau_g$ (leading to $t_{int} \simeq \tau_A$), where $\tau_g = m/(qB_0)$ is the gyro-period and $\tau_A = 2x_0/v_A$ is the Alfvén transit time. The energy spectra are obtained with 10^4 initially mono-energetic ($|\mathbf{v}_0| = 10^{-3} v_A$) particles, initiated in arbitrary directions with random coordinates within $x \in [-1:1]$ and $y \in [-2:2]$. The electromagnetic structure is assumed to be invariant for the time integration in the z-direction.

3 MHD simulation results

3.1 Typical evolution

The typical behaviour of the system is obtained through four successive DTM phases as illustrated in Fig. 1 (for $\eta = 5 \times 10^{-5}$) using the magnetic field lines. In order to measure the growth rate of DTM instabilities, we use the maximum absolute value of velocity y-component ($v_{y,max}$) in the domain, and its typical evolution is shown in Fig. 2. We are particularly interested in the explosive phase which is characterized by the coalescence of two initial magnetic islands (see Fig. 1-c and the time interval $200 \leq t \leq 250$ in Fig. 2). During this phase, the velocity $v_{y,max}$ increases very dynamically with an instantaneous growth rate, $v_{y,max} \propto e^{\sigma(t) \cdot t}$, where $\sigma(t)$ is the growth rate defined as $d\ln(v_{y,max})/dt$. Note that we have obtained $\sigma(t) \simeq \alpha t + \beta$ (α and β are constants), illustrating the explosive character of the phase.

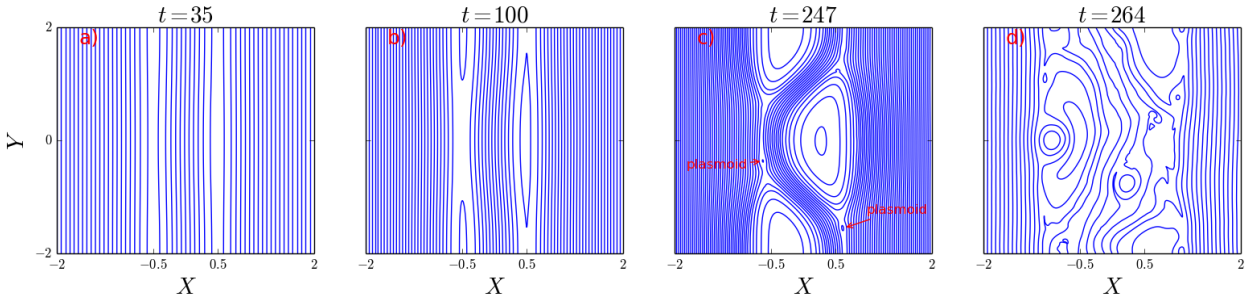

Fig. 1. Typical DTM evolution for $\eta = 5 \times 10^{-5}$: Magnetic filed lines corresponding to different phases of the DTM development (see Fig. 2). The explosive phase is represented in panel (c) at a given time where plasmoids are visible.

3.2 Scaling law with η

Since the growth rate σ evolves with time, one can measure the average and maximum growth rates of the explosive phase. This is done for different resistivity values in the range $[\,2 \times 10^{-6} : 2.5 \times 10^{-4}]$. Fig. 3 shows these results. As an important point, we obtained that the maximum rate (σ_{max}) increases very weakly with the resistivity as $\sigma_{max} \sim \eta^{0.05 \pm 0.04}$ (bottom panel of Fig. 3). In other words, σ_{max} is nearly independent of η. Moreover, secondary islands or "plasmoids" can be observed during this phase for cases where the local Lundquist number ($S_c = l v_A/\eta$ with a current sheet length l) exceeds a critical value, $S_c \gtrsim 10^4$, in agreement with theory [Loureiro et al. (2007)]. However, they appear as transient structures and disappear during the coalescence of primary islands. Consequently, they do not affect the explosive reconnection phase.

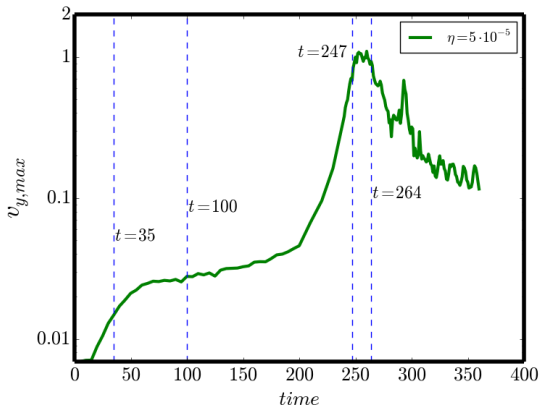

Fig. 2. Typical DTM evolution for $\eta = 5\times10^{-5}$: maximum value of $|\mathbf{v}_y|$ as a function of time. The times corresponding to panels of Fig. 1 are indicated by vertical lines.

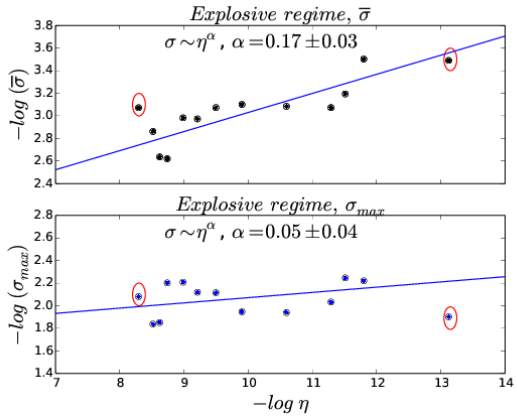

Fig. 3. Average (top panel) and maximum (bottom panel) measured growth rates of the explosive phase, as a function of the resistivity value. The two extreme points (with circles) are excluded from the linear fit.

4 Test-particle calculation results

In order to evaluate the efficiency of particle acceleration during the DTM phase, we have obtained energy spectra using 10^4 particles at different MHD times. Firstly, the so-called "saturation phase" (see Fig. 1-b and the time interval $80 \leq t \leq 180$ in Fig. 2) is chosen for comparison. The spectrum for this phase is plotted on left panel of Fig. 4. Secondly, the explosive phase is investigated at three different times ($t = 241, 247$ and 250). The results are shown on right panel of Fig. 4. One can see the considerable non-thermal acceleration ($3-4$ orders of magnitude higher in kinetic energy) process potentially contributing to the resulting synchrotron radiation with a spectral index of 1.75. The conclusion holds whatever is the resistivity value.

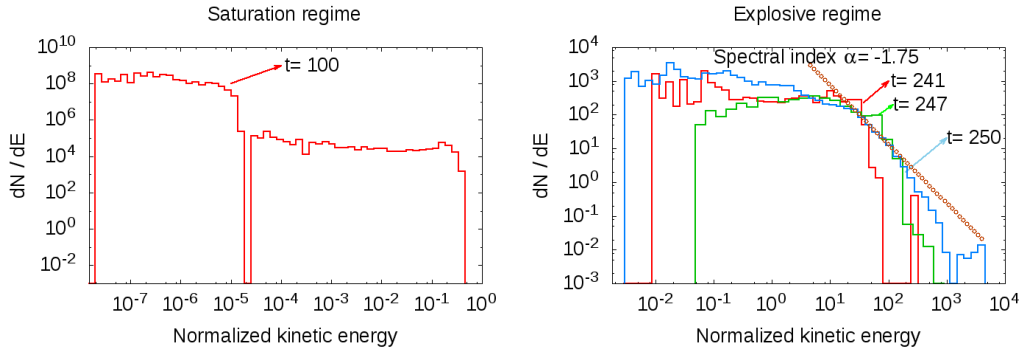

Fig. 4. Energy spectra obtained for the saturation phase at $t = 100$ (left panel) and for the explosive phase at $t = 241, 247, 250$ (right panel), using MHD configuration for a simulation with $\eta = 5\times10^{-5}$.

5 Conclusion

Our MHD results confirm the robustness of the DTM mechanism due to the very weak resistivity dependence of the explosive instabilty. Our results of test-particle acceleration show that an important non-thermal energization could also contribute to the resulting synchrotron radiation in addition to the thermal component (see synthetic synchrotron spectra obtained by Takamoto et al. (2015) in highly relativistic regime). Thus, the DTM instability of the magnetic structure in the striped wind region is a viable mechanism to explain Crab MeV flares. As the present results were obtained with newtonian MHD, we are actually extending our work to the more relevant relativistic MHD regime.

H. Baty acknowledges support by French National Research Agency (ANR) through Grant ANR-13-JS05-0003-01 (Project EMPERE). We also acknowledge computational facilities available at Equip@Meso of the Université de Strasbourg.

References

Baty, H., Petri, J., & Zenitani, S. 2013, MNRAS, 436, L20

Clausen-Brown, E. & Lyutikov, M. 2012, MNRAS, 426, 1374

Coroniti, F. V. 1990, ApJ, 349, 538

Loureiro, N. F., Schekochihin, A. A., & Cowley, S. C. 2007, Physics of Plasmas, 14, 100703

Lyutikov, M. 2003, MNRAS, 346, 540

Porth, O., Xia, C., Hendrix, T., Moschou, S. P., & Keppens, R. 2014, ApJs, 214, 4

Striani, E., Tavani, M., Vittorini, V., et al. 2013, ApJ, 765, 52

Takamoto, M., Pétri, J., & Baty, H. 2015, MNRAS, 454, 2972